Cancer Investigation, 27:496–503, 2009
ISSN: 0735-7907 print / 1532-4192 online

DOI: 10.1080/07357900802620836

informa
healthcare

ORIGINAL ARTICLE
Cellular and Molecular Biology

Expression Order of *Alpha-v* and *Beta-3* Integrin Subunits in the *N*-Methyl-*N*-Nitrosourea-Induced Rat Mammary Tumor Model

Robabeh Rezaeipoor,[1] Eric J. Chaney,[1] Amy L. Oldenburg,[1] and **Stephen A. Boppart[1,2]**

Beckman Institute for Advanced Science and Technology[1] and Departments of Electrical and Computer Engineering, Bioengineering, and Internal Medicine,[2] University of Illinois at Urbana-Champaign, Urbana, Illinois, USA

ABSTRACT

We investigated the developmental time course of molecular expression of $\alpha_v\beta_3$ subunits in a carcinogen-induced rat mammary tumor model for human ductal carcinoma *in situ* (DCIS). Tumors during various stages of growth (from <0.1 to >2.0 cm) were analyzed immunohistochemically for the expression of the $\alpha_v\beta_3$ integrin and its subunits. In general, the expression profiles of these integrin subunits were directly proportional to the size of the tumor. The pattern of immunostaining revealed that anti-$\alpha_v\beta_3$ monoclonal antibody binds to specific sites of tumor sections, forming isolated stained patches. This isolated patch pattern was found in more developed larger tumors. This could be due to the fact that the integrin molecule might be involved in migration and nesting of tumor cells into specific regions to form DCIS or intraductal carcinoma. Results also showed that the α_v subunit expresses earlier than the β_3 subunit. These data provide insight into tumor cell biology and developmental characteristics that will guide the future construction and use of targeted contrast and therapeutic agents capable of tracking, imaging, or treating a tumor at the earliest stage of formation.

INTRODUCTION

The development of molecular imaging technologies is complemented by increasing our fundamental understanding of the molecular biology of our targets. Targeting cells associated with cancer and angiogenesis using multifunctional agents coated with specific antibodies against tumor antigens (tumor markers) will subsequently lead to more effective tracking, imaging, and therapeutic measures.

Integrins are a family of cell surface receptors that mediate adhesion to a wide range of ligands present within the extracellular matrix or on the surface of opposing cells. Integrin activation controls cell adhesion, migration, and extracellular matrix assembly, thereby contributing to processes such as angiogenesis, cell proliferation, apoptosis, tumor cell metastasis, inflammation, the immune responses, and homeostasis (1–3). Structurally, integrins are heterodimers composed of noncovalently associated *alpha* and *beta* subunits. There are over 25 known integrin receptors. One integrin receptor that promises to be an effective target for molecular imaging of cancer because of its role in angiogenesis is the $\alpha_v\beta_3$ integrin, also called the vitronectin receptor. The $\alpha_v\beta_3$ integrin is expressed during angiogenesis and has been shown to correlate with tumor grade (4). It is typically overexpressed on various malignant tumors as well as on endothelial cells during neovascularization (5), in comparison to normal epithelium. The $\alpha_v\beta_3$ integrin is also found on normal platelets, neutrophils, and endothelial and epithelial cells. Co-binding of $\alpha_v\beta_3$ on aggressive metastatic cancer cells with platelets usually occurs. This is believed to lead to the attachment of circulating tumor cells to a thrombus of platelets and the establishment of a new colony (metastasis). Many investigators have studied the correlation between different integrin receptor expressions and tumor formation, metastasis, and prognosis (6–9).

To our knowledge, there has been no study that shows the time course of the molecular expression of the $\alpha_v\beta_3$ integrin and

Keywords: Alpha-v beta-3 subunits, Integrin, Expression, Breast cancer, Mammary tumors, Molecular Imaging
Correspondence to:
Stephen A. Boppart, MD, PhD
Beckman Institute for Advanced Science and Technology
405 North Mathews Avenue
Urbana, IL 61801, USA
email: boppart@illinois.edu

its subunits in breast cancer. Investigating and characterizing this time course will directly affect our strategies for functionalizing contrast and therapeutic agents and targeting them to tumors at various stages of growth. Thus, in this study, we designed a controlled experimental approach for mammary tumor formation in an inbred rat model using a widely utilized carcinogen, *N*-methyl-*N*-nitrosourea (MNU). Weekly, after carcinogen administration, a group of three inbred rats was killed and examined for any early sign of mammary tumor formation. Dissected tumors were found in a wide range of sizes, from very small (<0.1 cm) to well established (>2.0 cm). All of the collected samples were used for immunohistochemical analysis using monoclonal antibodies against α_v, β_3, and $\alpha_v\beta_3$ to quantify the expression profiles of these tumor markers. Based on our previous research using nanoparticles and microspheres for tracking and imaging tumor cells (10–12), having knowledge of the time-dependent expression profiles and expression levels of these cancer markers will aid in developing effectively targeted particles. More generally, this knowledge will aid in designing imaging protocols in clinics for oncology investigations (13) using any one of the molecular imaging modalities such as MRI (14–17), optical coherence tomography (OCT) (18, 19), PET, ultrasound, and near-infrared fluorescence imaging technologies (20–22).

MATERIALS AND METHODS

Animal model

Thirty-six Wistar–Furth female inbred rats (32 days old) (Jackson Labs, Bar Harbor, ME, USA) were used in this study. Experiments were performed in compliance with an experimental protocol approved by the Institutional Animal Care and Use Committee at the University of Illinois at Urbana-Champaign. The rats were individually housed, fed standard rat chow pellets, and provided with water and food *ad libitum*. Rats were kept on a 12-hr light–dark cycle and housed in the Biological Resources Facility at the Beckman Institute for Advanced Science and Technology at the University of Illinois At Urbana-Champaign.

Mammary tumor induction

N-methyl-*N*-nitrosourea (MNU) (50 mg/kg body weight), a carcinogen known to induce mammary tumors in rodents, was injected intraperitoneally (i.p.) twice, at a 1-week interval. The first injection was made in the left side and the second injection in the right side of the peritonea. For a negative control, a group of three Wistar rats were kept under the same housing conditions but with no MNU injection, receiving only an i.p. injection of the carrier buffer (0.9% NaCl, pH 4.0). Following MNU or control injections, animals were palpated weekly to determine mammary tumor development.

Sampling and tissue sectioning

For tumor sampling, rats were euthanized by CO_2 inhalation. Animals were then dissected and a whole mount of mammary tissue, regional lymph nodes, and any possible tumor [from very early stage (<0.1 cm) up to late stage (2.2 cm)] were resected. Tumor dimensions were measured by Fowler Calipers (Fred V. Fowler Co., Newton, MA, USA). The collected samples were placed in a freezing box containing isopropanol to control the rate of temperature decline and left at −80°C overnight. Subsequently, the samples were transferred into liquid nitrogen for long-term preservation. Whole mounts of mammary tissue were kept at −80°C. The frozen tissues were cryosectioned, with a thickness of 5 μm, using a Leica CM 3050 S Cryostat (Heidelberger Strusse, Nussloch, Germany). Thin cryosections were overlaid on poly-l-lysine-precoated slides (Histology Control Systems, Inc., Fisher, St. Louis, MO, USA), dried at room temperature for 30 min, and fixed with cold acetone for 15 min at 4°C. For longer preservation, the fixed sections were kept at −80°C before usage.

Cell lines

Human umbilical vein endothelial cells (HUVEC) (Cambrex Bio Science Walkersville, Inc.) were used as a positive cell line for the $\alpha_v\beta_3$ integrin.The HUVEC cell line was grown using the EGM-2 BulletKit (CC-3162) (Cambrex Bio Science Walkersville, Inc., East Rutherford, NJ, USA). Cell monolayers were grown on sterile round microscope cover slips (Fisher brand), which were placed in sterile Petri dishes containing specific cell culture media. Defined numbers of cells (typically approximately 10^6) were added into the corresponding media. Twenty-four hours after cell growth, the cover slips were washed three times using PBS. Then cells were fixed with cold acetone for 15 min at 4°C and kept at −20°C for subsequent immunochemical analysis using the appropriate primary and secondary antibodies to perform indirect solid-phase fluoroimmunoassays. A human breast adenocarcinoma cell line (SKBR-3) (ATCC) was used as a control (nonoverexpressed cell line) for $\alpha_v\beta_3$ integrin. The SKBR-3 cell line was grown in McCoy's 5A medium (modified) (ATCC) at 37°C in a humidified CO_2 incubator (5% CO_2 and 95% air). The cell monolayer formation and staining were performed exactly as described for the HUVEC cells.

Specific monoclonal antibodies

Mouse IgG1 monoclonal anti-α_v (Cat. No. GTX16821), anti-β_3 (Cat. No. GTX40146), and anti-$\alpha_v\beta_3$ (Cat. No. GTX40143) (Gene Tex, Inc., San Antonio, TX, USA) were used as primary antibodies.

Subsequently, fluorescein-5-isothiocyanate (FITC-isomer 1) conjugated to donkey antimouse IgG (H+L) with minimal cross-reactivity to rat was used as a secondary antibody (Lot No. 71524, Jackson ImmunoResearch Laboratories, Inc., West Grove, PA, USA).

Immunochemical analysis

To detect the subunit expression profiles from early tumor formation up to late-stage tumors, 5-μm-thick adjacent cryosections were made for all of the collected tumors and used for immunostaining. All sections were preblocked with 10% normal donkey serum (in PBS + 1% BSA) for 30 min at room temperature in a humid box. After blocking, the sections were washed

3×2 min using the washing buffer (PBS + 0.1% Tween 20). Then each section was incubated with the proper monoclonal antibodies (approximately 5 μg/mL) for 90 min at room temperature using the humid box. The sections were subsequently washed 3×2 min using the washing buffer. After washing, fluorescein-conjugated secondary antibody (1/100 dilution) was added to each section, incubated for 60 min in the humid box, then washed 3×2 min using the washing buffer. A drop of a hard set mounting medium (Vectashield, Vector Laboratories, Inc.) with (H-1200) or without (H-1400) propidium iodide (PI) was used for each fluoroimmunostained section and then covered with a cover slip and kept at 4°C for subsequent studies using fluorescent microscopy (Axiovert 200, Carl Zeiss, Germany).

Qualification and quantification analysis of immunofluorescence data

All of the fluoroimmunostained sections were studied by the same immunologist (R.R.) for qualification and scoring using fluorescence microscopy. The scoring was performed blinded and was also verified by a second investigator while performing the quantitative immunochemical analysis. Expression of the tumor markers either on the samples or on the negative controls were scored as completely negative (–), very low (±), low (+), intermediate (++), high (+ + +), and very high (+ + ++). To obtain the relative fluorescence intensity for each tumor marker expression during tumor formation and tumor growth, quantitative analysis was performed using MATLAB (The MathWorks, Inc., Natick, MA, USA) and ENVI (ITT Corporation, Boulder, CO, USA) software. The degree of expression of each tumor marker was quantified by analyzing image intensity profiles. We assume that there is a direct correspondence between the number of bright points (pixels) in a fluorescence image and the degree of expression of each integrin subunit. Image histograms were computed and intensity thresholds were chosen and set uniformly for each fluorescence image. A Lloyd–Max quantizer was first used to estimate the approximate value of the threshold. This method works well if there are distinct bright and dark regions, resulting in bimodal histograms. In cases where the histograms are not distinctly bimodal, the thresholds were chosen manually, with the Lloyd–Max threshold as the starting point, so as to include all bright regions and also such that any further change in threshold would result in the background being included. The number of pixels having intensity values higher than this threshold was computed for each image. Using the equation:

$$\%\text{fluorescence} = 100 \times (\text{number of pixels higher than threshold/total number of pixels}),$$

the percent fluorescence intensity was subsequently computed.

RESULTS AND DISCUSSION

Tumor induction

In this study, tumors of the same size induced at different times after carcinogen injection were examined for tumor marker expression. Typically, the induction of visible tumors in this experimental model occurred 6–8 weeks after carcinogen injection. We harvested the mammary tissues exactly 1 week after carcinogen injection, and continued this for other animals on a weekly basis, prior to any visible mammary tumor formation. Mammary tumors became visible to the eye at approximately 6 weeks. Whole mount preparations of mammary tissues were prepared and stained with H&E. There was epithelial cell proliferation and dysplasia present before the visible small-sized tumor formation. Immunostaining for $\alpha_v\beta_3$ integrin and subunits was not performed on mammary whole-mount preparations, but was performed on every tumor when they became visible. The immunostaining results showed that the expression profiles did not appear significantly on very small-sized tumors (<0.2 cm), but increased in tumors 0.2 cm and larger. Further increases were noted in relative proportion to tumor size. The tumor marker expression correlated with tumor size but not with the time after MNU injection. Therefore, the terms *early* and *late* stages refer to the size of tumors (small or large) and not the time after carcinogen injection. The size of the tumors varied from less than 0.1 cm up to more than 2.0 cm (Table 1).

Table 1. Qualitative Fluoroimmunostaining Analysis of Different Integrin Subunits Expression for Increasing Tumor Size

Range of Tumor Size (cm)	Number of Tumors	Anti-αv	Anti-β3	Anti-αvβ3
Less than 0.1	8	–	–	–
0.10–0.25	6	+	–	–
0.26–0.50	17	+	±	±
0.51–0.80	17	+	+	+
0.81–1.00	11	++	+	+
1.01–1.40	2	+	++	+
1.41–1.60	3	+	++	+
1.61–2.00	1	++	+ + +	++
Larger than 2.0	1	++	+ + +	+ + +

Note: Scored as negative (–), very low (±), low (+), intermediate (++), high (+ + +), and very high expression (+ + ++).

Cell line immunostaining

All of the primary monoclonal antibodies used in this study had a known specificity and reactivity with the rat integrin molecule and its subunits. To scientifically validate this for this study, testing was performed on positive and negative cell lines. To verify the specificity and activity of the monoclonal antibodies, and also to find the proper working dilutions for both primary and secondary antibodies, the integrin-positive and integrin-negative cell lines were subjected to indirect solid-phase immunostaining. The results indicate that all monoclonal antibodies used in our assays had high specificity and activity toward the HUVEC positive cell line (Fig. 1), with little to no reactivity with the SKBR-3 control cell line.

Immunochemical analysis of tumor sections

Results showed that the α_v subunit expresses earlier than the β_3 subunit (Table 1 and Fig. 5). The spatial pattern of

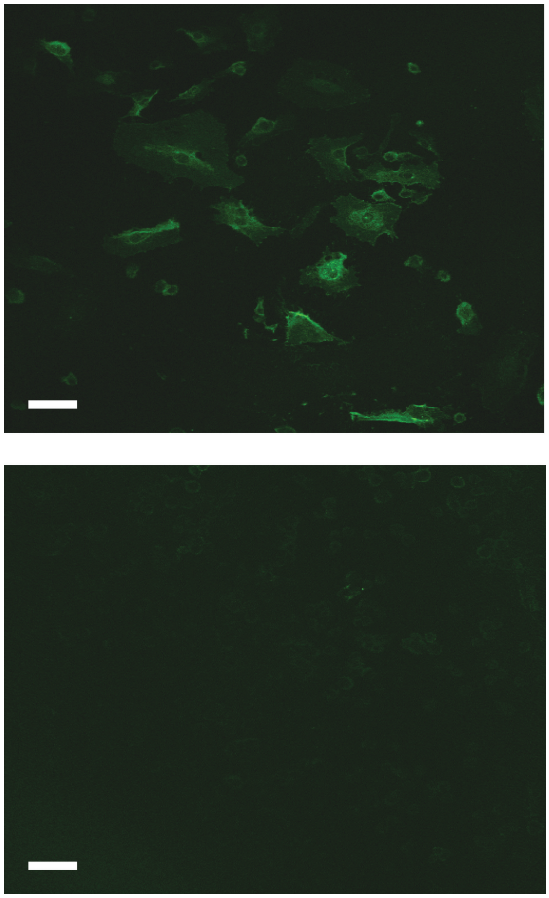

Figure 1. Fluoroimmunostaining of positive and negative control cell lines. Top: HUVEC (positive) and bottom: SKBR-3 (negative) control for the anti-$\alpha_v\beta_3$ antibody (20×, scale bar represents 50 μm).

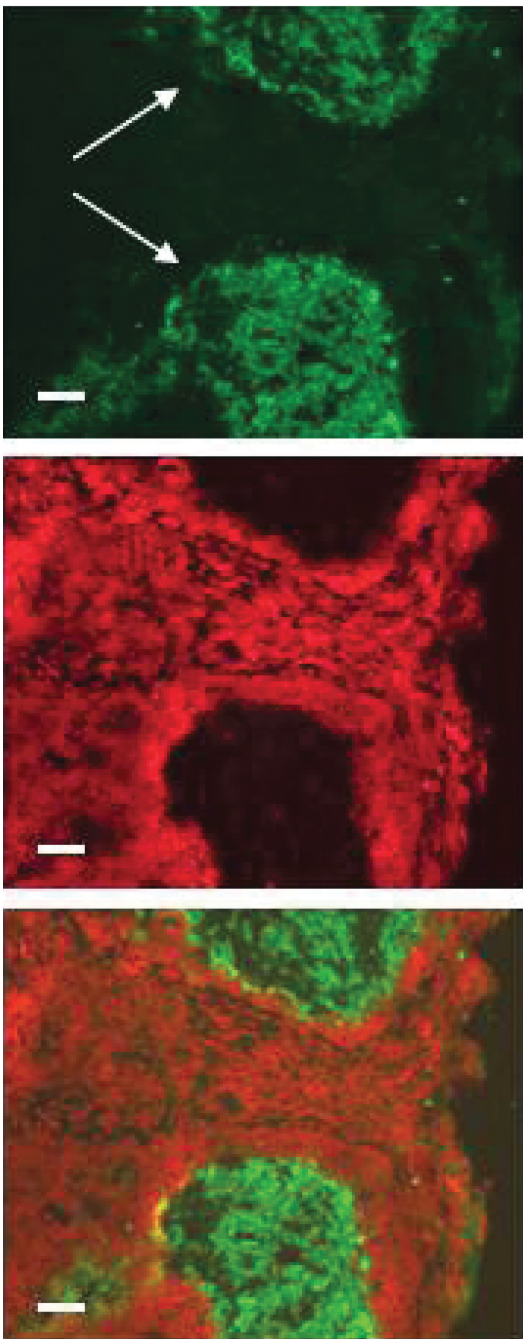

Figure 2. Fluoroimmunostaining of a 5-μm cryosection from a 2.0-cm rat mammary tumor using an anti-$\alpha_v\beta_3$ antibody. Arrows show the patch formation pattern after immunostaining (top). An adjacent cryosection stained with PI in mounting media (center). Overlay of top and center images (bottom) (20×, scale bar represents 50 μm).

immuno-staining revealed that anti-$\alpha_v\beta_3$ antibody binds to specific sites of tumor sections, forming isolated stained patches (Figure 2). After using the PI application in Fig. 2, we were not able to observe the stained nuclei of the tumor cells in the patch areas because the tumor sections were first treated with the primary monoclonal anti-integrin antibody and then treated with FITC-labeled secondary isotype-matched antiimmunoglobulin. Based on this coverage, and due to a masking effect, the PI could not penetrate to the tumor cell areas (patches) of the section because of steric hindrance. Hence, there was little to no red staining in these patch regions. In the indirect immunofluorescent assay applied for the immunochemical analysis, different antigenic determinants present on primary antibody molecules and recognized by secondary antibody molecules would eventually amplify the deposition of large quantities of antibody molecules mostly with the molecular weight of 150,000 Dalton. This kind of deposition will make a broad and impermeable barrier for any subsequent penetration, even for small-molecular-weight molecules such as PI (molecular weight of approximately 668.4 Dalton). However, under higher magnification of the patch areas, small disperse regions of red PI staining are evident, which are indicative of the presence of tumor cells in the patch areas (Fig. 2). This further demonstrates that the integrin molecule involved in this patch formation of tumor cells is localized to specific areas of the total tumor section.

The patch formation after immunostaining was also observed using the monoclonal anti-β_3 subunit antibody, while anti-α_v

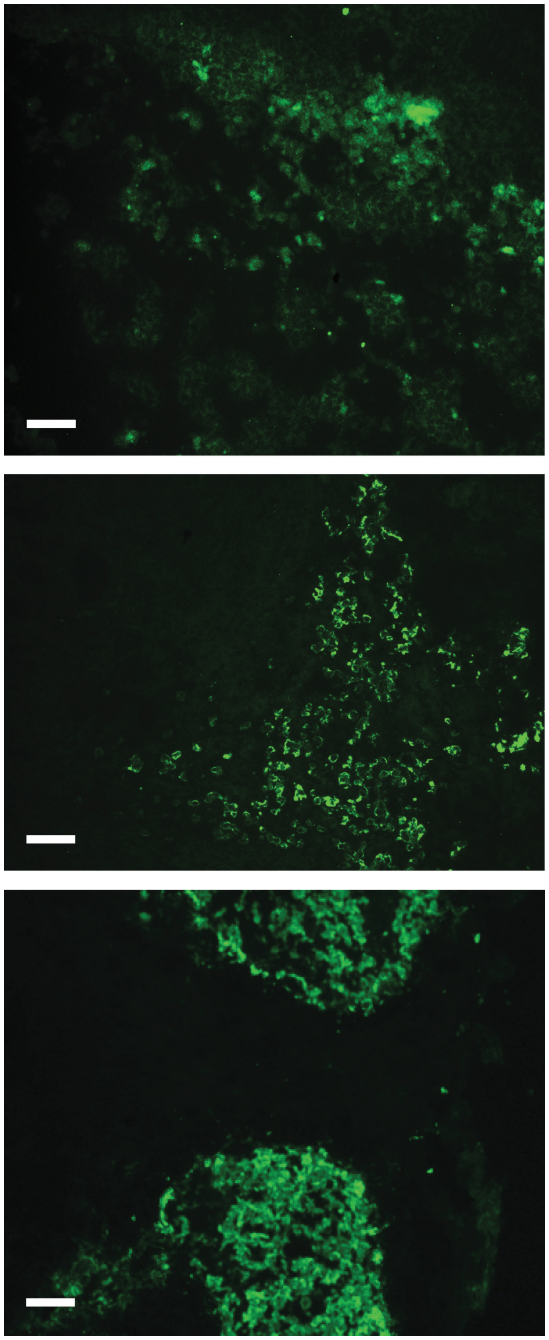

Figure 3. Tumor size-dependent progression of patch formation with $\alpha_v\beta_3$ integrin involvement. Fluorescence images of 5-μm cryosections of 0.5 cm (top), 1.0 cm (middle), and 2.0 cm (bottom) tumors after fluoroimmunostaining with an anti-$\alpha_v\beta_3$ antibody (20×, scale bar represents 50 μm).

showed a homogeneous pattern in immunostaining. The patch form of staining was found in more developed larger tumors (Fig. 3), which may be due to the fact that the integrin molecule, especially the β_3 subunit, is involved in migration of tumor cells into nesting sites to form DCIS or intraductal carcinoma. In accordance with the localization pattern it was also suggested

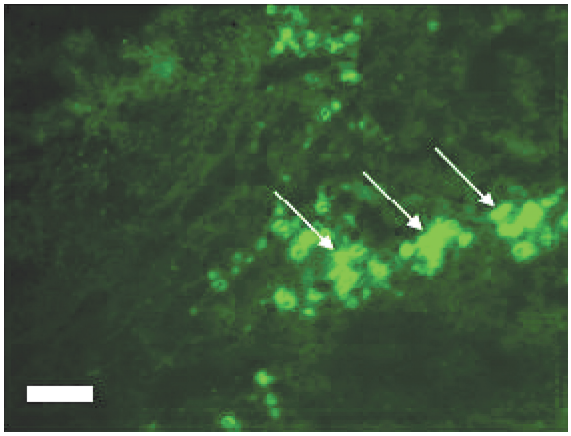

Figure 4. Fluorescence image of a 5-μm cryosection of a 2.0-cm tumor after fluoroimmunostaining with an anti-$\alpha_v\beta_3$ antibody. Arrows indicate new blood vessel formation (angiogenesis) in the large tumor (20×, scale bar represents 50 μm).

that the β_3 integrin is involved in tumor progression (23–25). In particular, the β_3 integrin, which is associated with a number of cancers, including prostate, cervical, breast, stomach, melanomas, and glioblastomas (26–31), has been recently targeted by a molecular probe (32). The anti-$\alpha_v\beta_3$ immunostaining also revealed the integrin involvement in angiogenesis, especially in larger tumors. Although it was observed that in addition to the nesting pattern of the tumor cells and subsequently the patch formation, the $\alpha_v\beta_3$ integrin was also involved in making new vessels supply the necessary nutrients for the new colony of tumor cells (Fig. 4).

The patch regions show the role of the integrin molecule in the selective homing pattern of tumor cells. We have used different monoclonal antibodies specifically to follow the expression pattern and order of $\alpha_v\beta_3$ integrin and its subunits. Because our main focus was not on angiogenesis, we did not use specific monoclonal antibodies that would target vessel markers such as CD31. However, the findings presented in Figure 4 are suggestive of vessel formation based on the morphological and spatial arrangements of the cells expressing the $\alpha_v\beta_3$ integrin, and further study is warranted.

Statistical analysis

For statistical analysis, because of small sample size, we used the Chi-square goodness-of-fit test. The results showed that the α_v subunit expresses earlier than the β_3 subunit ($p < .002$) (sample size 10). The expression of the α_v subunit with increasing tumor size was not significantly different ($p < .79$). However, the β_3 subunit and the $\alpha_v\beta_3$ integrin molecule had statistically meaningful increases in expression with larger tumor sizes ($p < .017$ and $p < .0000001$, respectively) (sample size 8).

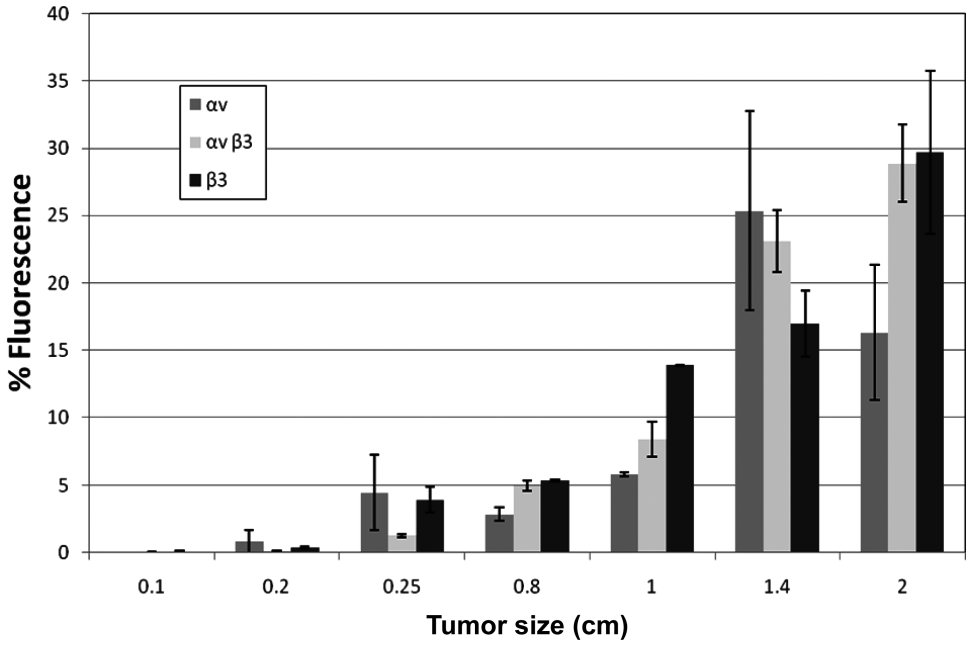

Figure 5. Relative expression levels for the $\alpha_v\beta_3$ integrin and its subunits with increasing tumor size. Chi-square statistical analysis showed that the α_v subunit expresses earlier than the β_3 subunit ($p < .002$) (sample size 10). The expression of the α_v subunit was not statistically meaningful with increasing tumor size ($p < .79$). However, the β_3 subunit and the $\alpha_v\beta_3$ integrin molecule had statistically meaningful increases in expression with larger tumor sizes ($p < .017$ and $p < .0000001$, respectively) (sample size 8).

Qualification and quantification analysis of immunochemical findings

Table 1 summarizes the qualitative scoring data for the expression of each tumor marker as correlated with tumor size. Using MATLAB and ENVI software, a subset of the immunochemical data were also analyzed quantitatively. The results showed that at a tumor size of 0.2 cm it is possible to detect early expression of the α_v subunit (Fig. 5). At this stage the β_3 subunit has not yet been expressed ($p < .002$, $N = 10$). The ability of the α_v subunit to combine with alternative *beta* subunits is well documented (33–35), which supports our finding that the α_v subunit is expressed earlier than β_3. Also, it has been shown that the α_v subunit influences conformation and ligand binding of $\alpha_v\beta_3$ (36). In another study (37), it was shown that M21 human melanoma variants lacking the α_v gene expression failed to express the integrin $\alpha_v\beta_3$ (M21-L cells). Thus, our finding about early expression of the α_v subunit is in agreement with the literature.

To our knowledge, this is the first documentation of the $\alpha_v\beta_3$ subunit expression in a breast cancer animal model. At the early stage of tumor formation where the α_v subunit was detected but not the β_3 subunit, we were not able to detect the $\alpha_v\beta_3$ integrin receptor. This shows that the specific monoclonal antibodies against $\alpha_v\beta_3$ are specific toward the bound heterodimer integrin receptor and are not capable of recognizing the subunit monomer. When the tumors became larger and the expression of β_3 gradually increased, it was observed that the α_v subunit could no longer be detected strongly using a monoclonal antibody against the α_v subunit. The main subunit of the $\alpha_v\beta_3$ integrin for binding to its specific ligand such as fibrinogen, fibrin, and vitronectin is the β_3 subunit (38). At larger tumor sizes (>1 cm), bound β_3 subunits are mostly observed, which may cause some form of a masking or blocking effect on the α_v subunit. Therefore, because of steric hindrance caused by the β_3 ligand binding, the specific antibody against α_v may not be capable of recognition and binding. Crosstalk among integrins, both positive and negative, is well established (39). The mechanisms, however, are not entirely clear, but are believed to include signal transduction and possibly competition for limiting components. It is completely clear, though, that integrins can affect functions of other integrins. Others have reported that binding of the $\alpha_v\beta_3$ receptor to its ligand, such as RGD, may block angiogenesis by inducing apoptosis (40–42). This may explain some of the downregulation observed for the integrin expression in our study, especially for the α_v subunit in the larger tumors. Although we did not study the dimerization of α_v with alternative β subunits, the relative changes of the β_3 subunit, compared to other β subunits throughout tumor development in this model is of interest, and will be part of future investigational studies.

CONCLUSIONS

To track and image tumor cells at the earliest stages of tumor formation, and ultimately eradicate them through different targeted means, requires a thorough understanding of the targeted receptors and their ligands. Further development of different tumor markers will provide better approaches for focusing

precisely on tumor cells at the right time and in the right place. The $\alpha_v\beta_3$ integrin receptor is the only one that binds to fibrinogen. This property of the integrin receptor, with the attachment of circulating tumor cells to a thrombus of platelets, may eventually cause the establishment of a new colony and is believed to be involved in tumor cell invasion and metastasis. Also, this integrin is essential for tumor survival through its role in providing a new blood supply for growing tumors (angiogenesis). Characterizing the expression profiles and spatial distributions of this receptor, as well as the timing of subunit expression, will provide essential information for tracking, imaging, and destroying tumor cells at early stages of development.

In this study, and for the first time, we have shown that in an animal model for human breast cancer, the α_v expresses earlier than the β_3 subunit. This suggests that targeting the α_v subunit may aid in identifying and treating breast cancer at an earlier stage. The time-dependent expression levels provide data that can subsequently be correlated with agent-targeting efficacy at various stages of tumor growth, and the spatial distribution of these tumor markers provides insight into how targeted contrast and therapeutic agents would localize in tumors, and ultimately distribute therapy spatially throughout the tumor and tissue. These results directly complement the development of targeted agents for identifying and tracking small tumors and even individual tumor cells *in vivo* using any one of the increasing number of molecular imaging modalities and techniques.

ACKNOWLEDGMENTS

We acknowledge helpful collaborative interactions with Prof. Samuel Achilefu from the Department of Radiology and Department of Biochemistry and Molecular Biophysics, Washington University School of Medicine, St. Louis, Missouri. We also wish to thank Dr. Rohit Bhargava and his graduate student Rohith K. Reddy from the Department of Bioengineering and the Beckman Institute for Advanced Science and Technology at the University of Illinois at Urbana-Champaign for their assistance in quantification of this data. This work was supported in part by the National Institutes of Health (Roadmap Initiative, NIBIB, 1 R21 EB005321 and 1 R01 EB005221, S.A.B.), and by NCI U54-CA119342-01 to the Siteman Center of Cancer Nanotechnology Excellence, through the University of Illinois Center for Nanoscale Science and Technology. Additional information can be found at http://biophotonics.uiuc.edu.

REFERENCES

1. Hynes, R.O. Integrins: bidirectional, allosteric signaling machines. Cell **2002**, *110*, 673–687.
2. Allen, C.M.; Sharman, W.M.; Madeleine, C.L.; Van Lier, J.E.; Weber, J.M. Attenuation of photodynamically induced apoptosis by an RGD containing peptide, Photochem Photobiol Sci **2002**, *1*, 246–254.
3. Ruoslahti, E. Fibronectin and its integrin receptors in cancer. Adv Cancer Res **1999**, *76*, 1–20.
4. Eliceiri, B.P.; Cheresh, D.A. The role of alpha v beta 3 integrins during angiogenesis. J Clin Invest **1999**, *103*, 1227–1230.
5. Boettiger, D.; Lynch, L.; Blystone, S.; Huber, F. Distinct ligand-binding modes for integrin $\alpha_v\beta_3$-mediated adhesion to fibronectin vs vitronectin. J Biol Chem **2001**, *276*(34), 31684–31690.
6. Maubant, S.; Cruet-Hennequart, S.; Dutoit, S.; Denoux, Y.; Crouet, H.; Amar, M.A.; Gauduchon, P. Expression of α_v-associated integrin β subunits in epithelial ovarian cancer and its relation to prognosis in patients treated with platinum-based regimens. J M Histol **2005**, *36*(1–2), 119–129.
7. Sigstad, E.; Dong, H.P.; Nielson, S.; Berner, A.; Davidson, B.; Rinsberg, B. Quantitative analysis of integrin expression in effusions using flow cytometric immunophenotyping. Diagn Cytopathol **2004**, *33*(5), 325–331.
8. Gui, G.P.; Wells, C.A.; Yeomans, P.; Jordan, S.E.; Vinson, G.P.; Carpenter, R. Integrin expression in breast cancer cytology: a novel predictor of axillary metastasis. Surg Oncol **1996**, *22*(3), 254–258.
9. Edlund, M.; Miyamoto, T.; Sikes, R.A.; Ogle, R.; et al. Integrin expression and usage by prostate cancer cell lines on laminin substrata. Cell Growth Differ **2001**, *12*(2), 99–107.
10. Boppart, S.A.; Oldenburg, A.L.; Xu, C.; Marks, D.L. Optical probes and techniques for molecular contrast enhancement in coherence imaging. J Biomed Opt **2005**, *10*(4), 0412081–04120814.
11. Oldenburg, A.L.; Toublan, F.J.J.; Suslick, K.S.; Wei, A.; Boppart, S.A. Magnetomotive contrast for *in vivo* optical coherence tomography. Opt Expr **2005**, *13*(17), 6597–6614.
12. Tobulan, F.J.J.; Boppart, S.A.; Suslick, K.S. Tumor targeting by surface-modified protein microspheres. J Am Chem Soc **2006**, *128*, 3472–3473.
13. Zysk, A.M.; Nguyen, F.T.; Oldenburg, A.L.; Marks, D.L.; Boppart, S.A. Optical coherence tomography: a review of clinical application development from bench to bedside. J Biomed Opt **2007**, *12*, 051403.
14. Artemov, D.; Mori, N.; Okollie, B.; Bhujwalla, Z.M. MR molecular imaging of the her-2/neu receptor in breast cancer cells using targeted iron oxide nanoparticles. Magn Reson Med **2003**, *49*, 403–408.
15. Funovics, M.A.; Kapeller, B.; Hoeller, C.; Su, H.; Kunstfeld, R.; Puig, S.; Macfelda, K. MR imaging of the her2/neu and 9.2.27 tumor antigens using immunospecific contrast agents. Magn Reson Imag **2004**, *22*, 0843–0850.
16. Aaron, J.S.; Oh, J.; Larson, T.A.; Kumar, S.; Milner, T.E.; Sokolov, K.V. Increased optical contrast in imaging of epidermal growth factor receptor using magnetically actuated hybrid gold/iron oxide nanoparticles. Opt Expr **2006**, *14*(29), 12930–12943.
17. Gruttner, C.; Muller, K.; Teller, J.; Westphal, F.; Foreman, A.; Ivkov, R. Synthesis and antibody conjugation of magnetic nanoparticles with improved specific power absorption rates for alternating magnetic field cancer therapy. J Magn Magn Mater **2007**, *311*, 181–186.
18. Lee, T.M.; Oldenburg, A.L.; Sitafalwalla, S.; Mark, D.L.; Luo, W.; Toublan, F.J.J.; Suslick, K.S.; Boppart, S.A. Engineered microsphere contrast agent for optical coherence tomography. Opt Lett **2003**, *28*(17), 1546–1548.
19. Oldenburg, A.L.; Crecea, V.; Rinne, S.A.; Boppart, S.A. Phase-resolved magnetomotive OCT for imaging nanomolar concentrations of magnetic nanoparticles in tissues. Opt Expr **2008**, *16*(15), 11525–11539. Magnetomotive contrast for *in vivo* optical coherence tomography. Opt Expr **2005**, *13*(17), 6597–6614.
20. Frangioni, J.V. Translating *in vivo* diagnostics into clinical reality. Nat Biotechnol **2006**, *24*, 909–913.
21. Li, C.; Wang, W.; Wu, Q.; Ke, S.; Houston, J.; Sevick-Muraca, E.; Dong, L.; Chow, D.; Charnsangavej, C.; Gelovani, J.G. Dual optical and nuclear imaging in human melanoma xenografts using a single targeted imaging probe. Nucl Med Biol **2006**, *33*, 349–358.
22. Adams, K.E.; Ke, S.; Kwon, S.; Liang, F.; Fan, Z.; Lu, Y. Comparison of visible and nearinfrared wavelength excitable fluorescent dyes for molecular imaging of cancer. J Biomed Opt **2007**, *12*, 024017.

23. Van Belle, P.A.; Elennitsas, R.; Satyamoorthy, K.; et al. Progression related expression of beta3 integrin in melanomas. Hum Pathol **1999**, *30*, 562–567.

24. Switala-Jelen, K.; Dabrowska, K.; Opolski, A.; Lipinska, L.; Nowaczyk, M.; Gorski, A. The biological functions of beta3 integrins. Folia Biol (Paraha) **2004**, *50*, 143–152.

25. Trikha, M.; Timar, J.; Zacharek, A.; Nemeth, J.A.; Cai, Y.L.; Done, B.; Somlai, B.; Raso. E.; Ladanyi, A.; Honn, K.V. Role for beta3 integrins in human melanoma growth and survival. Int J Cancer **2002**, *101*, 156–167.

26. Wang, X.; Ferreira, A.M.; Shao, Q.; Laird, D.W.; Sandig, M. Beta3 integrins facilitate matrix interactions during transendothelial migration of PC3 prostate tumor cells. Prostate **2005**, *63*, 65–80.

27. Gruber, G.; Hess, J.; Stiefel, C.; Aebersold, D.M.; Zimmer, Y.; Greiner, R.H.; Studer, U.; Altermatt, H.J.; Hlushchuk, R.; Djonov, V. Correlation between the tumoral expression of beta3-integrin and outcome in cervical cancer patients who had undergone radiotherapy. Br J Cancer **2005**, *92*, 41–46.

28. Pignatelli, M.; Cardillo, M.R.; Hanby, A.; Stamp, G. Integrins and their accessory adhesion molecules in mammary carcinomas. Hum Pathol **1992**, *23*, 1159–1166.

29. Kawahara, E.; Ooi, A.; Nakanishi, I. Integrin distribution in gastric carcinoma: association of beta3 and beta5 integrins with tumor invasiveness. Pathol Int **1995**, *45*, 493–500.

30. Albeda, S.M.; Mette, S.A.; Elder, D.E.; Stewart, R.; Damjanovich, L.; Herlyn, M.; Buck, C.A. Integrin distribution in malignant-melanoma: association of the beta3 subunit with tumor progression. Cancer Res **1990**, *50*, 6757–6764.

31. Gingras, M.C.; Roussel, E.; Bruner, J.M.; Branch, C.D.; Moser, R.P. Comparison of cell adhesion molecule expression between glioblastoma multiforme and autologous normal brain tissue. J Neuroimmunol **1995**, *57*, 143–153.

32. Bloch, S.; Xu, B.; Ye, Y.; et al. Targeting beta-3 integrin using a linear hexapeptide labeled with a near-infrared fluorescent molecular probe. Mol Pharm **2006**, *3*(5), 539–549.

33. Krissansen, G.W.; Elliott, M.J.; Lucas, C.M.; Stomski, F.C.; Berndt, M.C.; Cheresh, D.A.; Lopez, A.F.; Burns, G.F. Identification of a novel integrin α_v subunit expressed on cultured monocytes (macrophages). J Biol Chem **1990**, *265*, 823–830.

34. Cheresh, D.A.; Smith, J.; Cooper, H.; Quaranta, V. A novel vitronectin receptor integrin is responsible for distinct adhesive properties of carcinoma cells. Cell **1989**, *57*, 59–69.

35. Filardo, E.J.; Cheresh, D.A. A β turn in the cytoplasmic tail of the integrin α_v subunit influences conformation and ligand binding of $\alpha_v\beta_3$. J Biol Chem **1997**, *269*(6), 4641–4647.

36. Felding-Habermann, B.; Mueller, B.M.; Romerdahl, C.A.; Cheresh, D.A. Involvement of integrin alpha v gene expression in human melanoma tumorigenicity. J Clin Invest **1992**, *89*(6), 2018–2022.

37. Albelda, S.M.; Mette, S.A.; Elder, D.E; Stewart, R.M; Damjanovich, L.; Herlyn, M.; Clayton, A. Integrin distribution in malignant melanoma. Cancer Res **1990**, *50*, 6757–6764.

38. Blystone, S.D.; Slater, S.E.; Williams, M.P.; Crow, M.T.; Brown, E.J. A molecular mechanism of integrin crosstalk. J Cell Biol **1999**, *145*, 889–897.

39. Schwartz, M.A.; Ginsberg, M.H. Networks and crosstalk: integrin signalling spreads. Nat Cell Biol **2002**, *4*, E65–E68.

40. Brooks, P.C.; Montgomery, A.M.; Rosenfeld, M.; Reisfeld, R.A.; Hu, T.; Klier, G.; Cheresh, D.A. Integrin $\alpha_v\beta_3$ antagonists promote tumor regression by inducing apoptosis of angiogenic blood vessels. *Cell* **1994**, *79*(7), 1157–1164.

41. Brooks, P.C.; Strömblad, S.; Klemke, R.; Visscher, D.; Sarkar, F.H.; Cheresh, D.A. Anti-integrin alpha v beta 3 blocks human breast cancer growth and angiogenesis in human skin. J Clin Invest **1995**, *96*(4), 1815–1822.

42. Friedlander, M.; Brooks, P.C.; Shaffer, R.W.; Kincaid, C.M.; Varner, J.A.; Cheresh, D.A. Definition of two angiogenic pathways by distinct alpha v integrins. Science **1995**, *270*(5241), 1500–1502.